

The Szekeres Swiss Cheese model and the CMB observations

Krzysztof Bolejko^{1,2}

¹The University of Melbourne, Melbourne VIC 3010, Australia

²Nicolaus Copernicus Astronomical Center, Bartycka 18, 00-716 Warsaw, Poland
bolejko@camk.edu.pl

May 27, 2019

Abstract

This paper presents the application of the Szekeres Swiss Cheese model to observations of the cosmic microwave background (CMB) radiation. It aims to study the CMB temperature fluctuations by the means of the exact inhomogeneous Szekeres model. So far the impact of inhomogeneous matter distribution on the CMB observations has been almost exclusively studied within the linear perturbations of the Friedmann model. However, since the density contrast of cosmic structures is larger than 1 this issue is worth studying using another approach. The Szekeres model is an inhomogeneous, non-symmetrical and exact solution of the Einstein equations. In this model, light propagation and matter evolution can be exactly calculated, without approximations such as small amplitude of the density contrast. This will allow us to examine the impact of light propagation effects on the CMB temperature fluctuations.

The results of such analysis show that small-scale, non-linear inhomogeneities introduce — via light propagation effects — temperature fluctuations of amplitude $10^{-6} - 10^{-7}$. Since these temperature fluctuations are of one order of magnitude smaller than the observed value this means that the Rees-Sciama effect does not have a significant impact on the CMB data. On the other hand, local and uncompensated inhomogeneities can introduce temperature fluctuations of amplitude as large as 10^{-3} .

1 Introduction

The Universe, as it is observed, is quite inhomogeneous. Among the structures we observe in the Universe are clusters and superclusters of galaxies as well as large cosmic voids. This inhomogeneous matter distribution affects light propagation and hence astronomical observations. To estimate how light-propagation effects influence the results of astronomical observations, the homogeneous Friedmann models with linear perturbations are usually applied. However, since density fluctuations in the Universe are large, such analysis can lead to either underestimation or overestimation of the cosmological parameters. Therefore, there is a need for application of exact and inhomogeneous models to a study of the light propagation and its impact on astronomical observations. This issue has been extensively studied within spherically symmetric models. However, most of the cosmic structures are not spherically symmetric, and thus the study of light propagation in non-symmetrical models is essential. One of the suitable models for this purpose is the Szekeres model and its application to the CMB observations is presented in this paper.

The structure of this paper is as follows. Sec. 2 presents standard formulae describing light propagation; in Sec. 3 the Szekeres model is presented; Sec. 3.3 presents the null geodesics equations; Sec. 4 presents the construction of models; Sec. 5 presents the findings.

2 Light propagation

Light propagates along null geodesics. If k^α is a vector tangent to a null geodesic, then

$$k_\alpha k^\alpha = 0, \quad k_{\alpha;\beta} k^\beta = 0. \quad (1)$$

As light propagates, the frequency of photons changes. The ratio of the frequency of a photon at the emission event to the measured frequency defines the redshift

$$\frac{\nu_e}{\nu_o} := 1 + z. \quad (2)$$

As seen from the above definition, $(1+z)$ is a multiplicative quantity. For example, if there are many measurement along the light ray, and each observer measures the redshift and re-emits the light towards next observer, then the final redshift is given by

$$1+z = \frac{\nu_e}{\nu_o} = \frac{\nu_e}{\nu_1} \frac{\nu_1}{\nu_2} \dots \frac{\nu_{n-1}}{\nu_n} \frac{\nu_n}{\nu_o} = (1+z_1)(1+z_2)\dots(1+z_o). \quad (3)$$

On the other hand, since photon's energy, as measured by an observer with the 4-velocity u^α , is proportional to $k^\alpha u_\alpha$, thus the redshift obeys the following relation

$$1+z = \frac{(k^\alpha u_\alpha)_e}{(k^\alpha u_\alpha)_o}, \quad (4)$$

where the subscripts e and o refer to instants of emission and observation respectively.

Assuming that the black body spectrum is conserved during the evolution of the Universe, the temperature must be proportional to $1+z$

$$\frac{T_e}{T_o} = 1+z. \quad (5)$$

Then, from eq. (5), the temperature fluctuations measured by comoving observer are:

$$\left(\frac{\Delta T}{T}\right)_o = \frac{T_e/(1+z) - \bar{T}_e/(1+\bar{z})}{\bar{T}_e/(1+\bar{z})}, \quad (6)$$

where quantities with bars $\bar{}$ refer to average quantities. It will be assumed that the average quantities are equal to quantities obtained within the homogeneous Friedmann model.

Let us define the temperature at the emission point as, $T_e = \bar{T}_e + \Delta T_e$. Then eq. (6) becomes

$$\left(\frac{\Delta T}{T}\right)_o = \frac{1/(1+z) - 1/(1+\bar{z})}{1/(1+\bar{z})} + \left(\frac{\Delta T}{T}\right)_e \frac{1+\bar{z}}{1+z}. \quad (7)$$

As can be seen from the above formula, the observed temperature fluctuations on the CMB sky are caused by the light propagation effects (the first term) and by the temperature fluctuations at the decoupling instant (the second term — however this term is modified by light propagation effects).

3 The Szekeres model

3.1 The metric of the Szekeres model

For our purpose it is convenient to use a coordinate system different from that in which Szekeres [1] originally found his solution. The metric is of the following form [2]

$$ds^2 = c^2 dt^2 - \frac{(\Phi' - \Phi \frac{E'}{E})^2}{(\varepsilon - k)} dr^2 - \Phi^2 \frac{(dp^2 + dq^2)}{E^2}, \quad (8)$$

where $' \equiv \partial/\partial r$, $\varepsilon = \pm 1, 0$ and $k = k(r) \leq \varepsilon$ is an arbitrary function of r .

The function E is given by

$$E(r, p, q) = \frac{1}{2S}(p^2 + q^2) - \frac{P}{S}p - \frac{Q}{S}q + C, \quad (9)$$

where the functions $S = S(r)$, $P = P(r)$, $Q = Q(r)$, and $C = C(r)$ satisfy the relation

$$C = \frac{P^2}{2S} + \frac{Q^2}{2S} + \frac{S}{2}\varepsilon, \quad \varepsilon = 0, \pm 1, \quad (10)$$

but are otherwise arbitrary.

As can be seen from (8), only $\varepsilon = +1$ allows the model to have all three Friedmann limits (hyperbolic, flat, and spherical). This is induced by the requirement of the Lorentzian signature of the metric (8). As we are interested in the Friedmann limit of our model, i.e. we expect it becomes a homogeneous Friedmann model at a large distance from the origin, we will focus only on the $\varepsilon = 1$ case. This case is often called the quasispherical Szekeres model.

3.2 The Einstein equation

Applying metric (8) to the Einstein equations, and assuming the energy momentum tensor for a dust, the Einstein equations reduce to the following two

$$\frac{1}{c^2} \dot{\Phi}^2(t, r) = \frac{2M(r)}{\Phi(t, r)} - k(r) + \frac{1}{3} \Lambda \Phi^2(t, r), \quad (11)$$

$$4\pi \frac{G}{c^2} \rho(t, r, p, q) = \frac{M'(r) - 3M(r)E'(r, p, q)/E(r, p, q)}{\Phi^2(t, r)[\Phi'(t, r) - \Phi(t, r)E'(r, p, q)/E(r, p, q)]}. \quad (12)$$

In a Newtonian limit Mc^2/G is equal to the mass inside the shell of radial coordinate r . However, it is not an integrated rest mass but active gravitational mass that generates a gravitational field. The function $k(r)$ is another arbitrary function defining the Szekeres model. By analogy with the Newtonian energy conservation equation, eq. (11) shows that the function $(-k/2)$ represents the energy per unit mass of the particles in the shells of matter at constant r . On the other hand, by analogy with the Friedmann equation and from the metric (8) the function k determines the geometry of the spatial sections $t = \text{const}$. However, since k is a function of the radial coordinate, the geometry of the space is now position dependent.

Eq. (11) can be integrated

$$\int_0^{\Phi} \frac{d\tilde{\Phi}}{\sqrt{\frac{2M(r)}{\Phi} - k(r) + \frac{1}{3}\Lambda\tilde{\Phi}^2}} = c[t - t_B(r)], \quad (13)$$

where t_B is an arbitrary function of r . This means that the big bang is not a single event as in the Friedmann models but occurs at different times for different distances from the origin.

As can be seen the Szekeres model is specified by 6 functions. However, by a choice of the coordinates, the number of independent functions can be reduced to 5.

3.3 Null geodesic equations

As follows from eqs. (7) and (4), to compute the observed temperature fluctuations the geodesic equation (1) within a cosmological model must be solved. The geodesic equations

$$\frac{d^2 x^\alpha}{ds^2} + \Gamma_{\beta\gamma}^\alpha \frac{dx^\beta}{ds} \frac{dx^\gamma}{ds} = 0. \quad (14)$$

in the quasispherical Szekeres model, are:

$\alpha = 0$:

$$\frac{d^2 t}{ds^2} + \frac{\dot{\Phi}' - \dot{\Phi}E'/E}{1-k} (\Phi' - \Phi E'/E) \left(\frac{dr}{ds}\right)^2 + \frac{\Phi\dot{\Phi}}{E^2} \left[\left(\frac{dp}{ds}\right)^2 + \left(\frac{dq}{ds}\right)^2 \right] = 0, \quad (15)$$

$\alpha = 1$:

$$\begin{aligned} & \frac{d^2 r}{ds^2} + 2 \frac{\dot{\Phi}' - \dot{\Phi}E'/E}{\Phi' - \Phi E'/E} \frac{dt}{ds} \frac{dr}{ds} + \left(\frac{\Phi'' - \Phi'E'/E - \Phi E''/E + \Phi(E'/E)^2}{\Phi' - \Phi E'/E} + \frac{1}{2} \frac{k'}{1-k} \right) \left(\frac{dr}{ds}\right)^2 \\ & + 2 \frac{\Phi}{E^2} \frac{E'\partial_p E - E\partial_p E'}{\Phi' - \Phi E'/E} \frac{dr}{ds} \frac{dp}{ds} + 2 \frac{\Phi}{E^2} \frac{(E'\partial_q E - E\partial_q E')}{\Phi' - \Phi E'/E} \frac{dr}{ds} \frac{dq}{ds} \\ & - \frac{\Phi}{E^2} \frac{1-k}{\Phi' - \Phi E'/E} \left[\left(\frac{dp}{ds}\right)^2 + \left(\frac{dq}{ds}\right)^2 \right] = 0, \end{aligned} \quad (16)$$

$\alpha = 2$:

$$\begin{aligned} & \frac{d^2 p}{ds^2} + 2 \frac{\dot{\Phi}}{\Phi} \frac{dt}{ds} \frac{dp}{ds} - \left(\frac{1}{\Phi} \frac{\Phi' - \Phi E'/E}{1-k} (E'\partial_p E - E\partial_p E') \right) \left(\frac{dr}{ds}\right)^2 + 2 \left(\frac{\Phi'}{\Phi} - \frac{E'}{E} \right) \frac{dr}{ds} \frac{dp}{ds} \\ & - \frac{\partial_p E}{E} \left(\frac{dp}{ds}\right)^2 - 2 \frac{\partial_q E}{E} \frac{dp}{ds} \frac{dq}{ds} + \frac{\partial_p E}{E} \left(\frac{dq}{ds}\right)^2 = 0, \end{aligned} \quad (17)$$

$\alpha = 3$:

$$\begin{aligned} & \frac{d^2 q}{ds^2} + 2 \frac{\dot{\Phi}}{\Phi} \frac{dt}{ds} \frac{dq}{ds} - \left(\frac{1}{\Phi} \frac{\Phi' - \Phi E'/E}{1-k} (E'\partial_q E - E\partial_q E') \right) \left(\frac{dr}{ds}\right)^2 + 2 \left(\frac{\Phi'}{\Phi} - \frac{E'}{E} \right) \frac{dr}{ds} \frac{dq}{ds} \\ & + \frac{\partial_q E}{E} \left(\frac{dp}{ds}\right)^2 - 2 \frac{\partial_p E}{E} \frac{dp}{ds} \frac{dq}{ds} - \frac{\partial_q E}{E} \left(\frac{dq}{ds}\right)^2 = 0. \end{aligned} \quad (18)$$

4 Model set-up

4.1 Model specification

To define the Szekeres model five functions of radial coordinate are needed. In this paper all models will be defined by the following set of functions: k , M , S , P , and Q .

The algorithm used in the calculations can be defined as follows:

1. The radial coordinate is chosen to be the areal radius at the initial instant $r' = \Phi(r, t_i)$. However, for clarity in further use, the prim is omitted and the new radial coordinate will be referred to as r .
2. The chosen background model is the homogeneous Friedmann model with density at present instant

$$\rho_b = \Omega_m \times \rho_{cr} = 0.24 \times \frac{3H_0^2}{8\pi G}. \quad (19)$$

where the Hubble constant is $H_0 = 74 \text{ km s}^{-1} \text{ Mpc}^{-1}$. The cosmological constant, Λ , corresponds to $\Omega_\Lambda = 0.76$, where $\Omega_\Lambda = (1/3)(c^2\Lambda/H_0^2)$.

3. The initial time, t_i , is chosen to be the time of last scattering, and is calculated from the following formula for a background FLRW universe [3]

$$t(z) = \frac{1}{H_0} \int_z^\infty \frac{d\tilde{z}}{(1+\tilde{z})\sqrt{\mathcal{D}(\tilde{z})}}, \quad (20)$$

where:

$$\mathcal{D}(z) = \Omega_\gamma(1+z)^4 + \Omega_{mat}(1+z)^3 + \Omega_K(1+z)^2 + \Omega_\Lambda, \quad (21)$$

H_0 is the present Hubble constant, $\Omega_K = 1 - \Omega_\gamma - \Omega_{mat} - \Omega_\Lambda$. For the lower limit of integration, $z = 1089$ was used as the redshift at last scattering [4].

4. There will be three different Szekeres regions which will be used to construct the Swiss Cheese model. Let us denote them as regions a , b , and c . The functions M , k , Q , P and S in these regions are defined as follows

(a) Region a

$$M = M_0 + \delta M,$$

$$\delta M = \begin{cases} A_1 \ell^3 & \text{for } \ell \leq 0.5b, \\ A_2 \exp\left[-6\left(\frac{\ell-b}{b}\right)^2\right] & \text{for } \ell \geq 0.5b, \end{cases}$$

$$k = \begin{cases} A_3 \ell^2 & \text{for } \ell \leq 0.5a, \\ A_4 \exp\left[-\left(\frac{\ell-a}{0.5a}\right)^2\right] & \text{for } \ell \geq 0.5a, \end{cases}$$

$$S = 1,$$

$$P = 0,$$

$$Q = -0.22 \ln(1 + \ell) \times \exp(-0.1\ell). \quad (22)$$

where $\ell = r/\text{Kpc}$, M_0 is the mass in the corresponding volume of the homogeneous universe [i.e. $M_0 = (4\pi G/3c^2)\rho_{b,ls}r^3$, $\rho_{b,ls} = \rho_b(1+z_{ls})^3$], $A_1 = 8c^{-3}A_2e^{-1.5}$, $A_2 = -0.748588$, $b = 15.2272$, $A_3 = 4a^{-2}A_4e^{-1}$, $A_4 = -1.00173 \times 10^{-5}$, $a = 12.9495$.

(b) Region b

$$\delta M = \begin{cases} B_1 \ell^3 & \text{for } \ell \leq 0.5g, \\ B_2 \exp\left[-6\left(\frac{\ell-g}{g}\right)^2\right] & \text{for } \ell \geq 0.5g, \end{cases}$$

$$k = \begin{cases} B_3 \ell^2 & \text{for } \ell \leq 0.5f, \\ B_4 \exp\left[-\left(\frac{\ell-f}{0.5f}\right)^2\right] & \text{for } \ell \geq 0.5f, \end{cases}$$

$$S = 1,$$

$$P = 0,$$

$$Q = -1.4 \ln(1 + 0.4\ell) \times \exp(-0.005\ell). \quad (23)$$

where $B_1 = 8g^{-3}B_2e^{-1.5}$, $B_2 = 0.9$, $g = 23.7587$, $B_3 = 4f^{-2}B_4e^{-1}$, $B_4 = 5.056 \times 10^{-6}$, $f = 19.1$,

(c) Region c

$$\delta M = \begin{cases} C_1 \ell^3 & \text{for } \ell \leq 0.5g, \\ C_2 \exp \left[-6 \left(\frac{\ell-g}{g} \right)^2 \right] & \text{for } \ell \geq 0.5g, \end{cases}$$

$$k = \begin{cases} C_3 \ell^2 & \text{for } \ell \leq 0.5f, \\ C_4 \exp \left[- \left(\frac{\ell-f}{0.5f} \right)^2 \right] & \text{for } \ell \geq 0.5f, \end{cases}$$

$$\begin{aligned} S &= 1, \\ P &= 0, \\ Q &= -1.4 \ln(1 + 0.4\ell) \times \exp(-0.005\ell). \end{aligned} \quad (24)$$

where $C_1 = 8g^{-3}C_2e^{-1.5}$, $C_2 = 0.55$, $C_3 = 4e^{-2}C_4e^{-1}$, $C_4 = 3.6 \times 10^{-6}$.

Density distribution in region a at the current instant is presented in Fig. 1. Density distribution in region b at the current instant is presented in Fig. 2. The density distribution in region c is similar to the density distribution in region b except that at the origin the amplitude of density fluctuations is $\rho/\rho_b = 1.5$ instead of 2.5 as in region b .

It should be noted that left panels of Figs. 1 and 2 should be regarded as a schematic. These Figures were obtained in the following way: first coordinates (p, q) were transformed to the spherical coordinates [5]

$$\begin{aligned} p &= P + S \cot \frac{\vartheta}{2} \cos \varphi, \\ q &= Q + S \cot \frac{\vartheta}{2} \sin \varphi; \end{aligned} \quad (25)$$

then coordinates (ϑ, φ) were transformed to following coordinates:

$$\begin{aligned} X &= \Phi(t_0, r) \sin \vartheta \cos \varphi, \\ Y &= \Phi(t_0, r) \sin \vartheta \sin \varphi, \\ Z &= \Phi(t_0, r) \cos \vartheta. \end{aligned} \quad (26)$$

Thus, density distribution presented in left panels of Figs. 1 and 2 are distorted in two ways. The first source of distortion comes from the transformation (26) that assumes that all spheres have the same origin. The second source of distortion comes from the mapping of the XY -surface from curved spacetime to a 2 dimensional flat surface (such as a sheet of this paper). However, it is only a shape that is distorted and not the values of density.

Fig. 3 presents the bang time functions t_B in regions a , b , and c . As can be seen, the amplitude of t_B is never higher than 100 years, which in comparison with the age of the Universe at and after the decoupling instant is negligible.

4.2 Arrangement of the Swiss Cheese model

Let us consider the arrangement of the Swiss Cheese model. Its each region is matched into a Friedmann background, i.e. the functions defining the Szekeres model are such that at the distance around 40 Mpc they behave as in the Friedmann model. At this distance the model is joined with the Friedmann model. Such junction is possible because on the boundary surface defined by $\rho = \text{const}$ the 3D-metric of this surface and its second fundamental form are continuous. The only condition of such junction is that the mass inside the inhomogeneous region described by the Szekeres model is equal to the mass of the homogeneous background Friedmann model that would be contained in the same volume¹.

First null geodesic equations for one Szekeres region are solved. Then, after the exit from the Szekeres region at the point where the Szekeres model becomes the Friedmann model, photons immediately enter another inhomogeneous patch. Then again the null geodesics equations for this next region are solved.

Three different Swiss Cheese models are considered. In model 1 light propagates alternately through regions a and b . In model 2 light also propagates alternately through regions a and b . In model 3 light propagates alternately through regions a and c .

When the light ray enters another patch the following can be chosen

¹It might be surprising that a nonsymmetrical model like the Szekeres can be joined with the symmetric Friedmann model, but there are other examples of such junctions. For example Bonnor showed that the Szekeres model can be matched to the Schwarzschild solution [6].

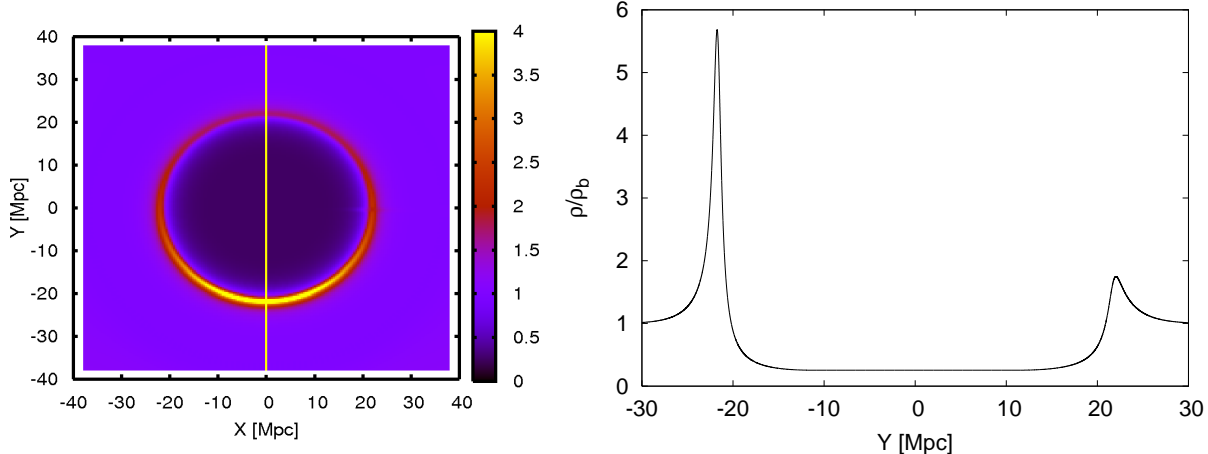


Figure 1: The density distribution ρ/ρ_b in region a at the present instant. Left panel presents the colour coded graph of density distribution on the surface $Z = 0$. The right panel presents the density distribution along the line shown in the left panel.

- the point where light enters the patch, and
- the initial direction along which light start to propagate (this is equivalent to choosing the orientation of the patch).

This freedom is exercised models 1–3 are specified. In model 1 the point where the light ray enters another patch is fixed. Only the initial direction along which the light ray starts to propagate is randomly chosen — this is equivalent to randomly choosing k^i . In model 2 the initial direction (k^i) is fixed. Only the point where the light ray enters the patch is randomly selected. Model 3 is similar to model 2 but instead of patch b , patch c is used.

Light propagation was calculated by solving eqs. (1) simultaneously with the evolution equation (11). This was done using the fourth order Runge–Kutta method. In model 1 initial conditions are: $r_a = 40$ Mpc, $r_b = 50$ Mpc, (where a, b, c label the regions), the initial values of p, q correspond to $\theta = \pi/2$, $\phi = \pi/6$ [see the transformation (25)]. $k^0 = 1$, initial values of k^3 and k^4 are randomly selected, k^1 is then calculated from $k_\alpha k^\alpha = 0$.

Initial conditions in model 2 are: $r_a = 40$ Mpc, $r_b = 50$ Mpc, (a, b, c correspond to regions), initial values of p, q are then randomly selected. Initial values of k^μ in region a are: $k^0 = 1$, $k^3 = 10^{-6}$ i $k^4 = 0$; in region b : $k^0 = 1$, $k^3 = 0$ i $k^4 = 10^{-6}$.

The initial conditions in model 3 are: $r_a = 40$ Mpc, $r_c = 50$ Mpc, other values as in model 2.

5 Results

5.1 The Rees-Sciama effect

Temperature fluctuations caused by light propagation effects are presented in Fig. 4. These temperature fluctuations were calculated from eq. (7). The redshift in each region was calculated separately from eq. (4). The total redshift was calculated from eq. (3): $(1+z) = (1+z_a)(1+z_x)(1+z_a)\dots(1+z_x)$ (where x is b in model 2 or c in model 3). The mean redshift \bar{z} was calculated in Λ CDM model.

As is seen in Fig. 4, the final values are small, of amplitude $\Delta T/T \approx 10^{-7}$ (curves 1, 2 and 3). Detailed analysis of how inhomogeneities cause temperature fluctuations is presented in Fig. 5 (for clarity, only a small fraction of the time is presented). The left panel of Fig. 5 shows the density of regions through which the light propagates in model 1. The right panel presents the temperature fluctuations as measured by an observer situated just behind an inhomogeneous patch in the homogeneous region. Letters correspond to each inhomogeneous patch (left panel) and temperature fluctuations caused by them (right panel). As can be seen, underdense regions induce negative temperature fluctuations, overdense regions induce positive fluctuations. Since each underdense region (a) is followed by an overdense region (b or c), the final values are small. When light is propagated mostly through underdense regions (a regions — curve a in Fig. 4) or overdense regions (b regions — curve b in Fig. 4), the final values are higher by one order of magnitude, i.e. $\Delta T/T \approx 10^{-6}$.

5.2 The role of local structures

So far, it has been assumed that each inhomogeneous structure is compensated (i.e. each Szekeres region was matched with the Friedmann background), and that measurements are carried out away from the inhomogeneities,

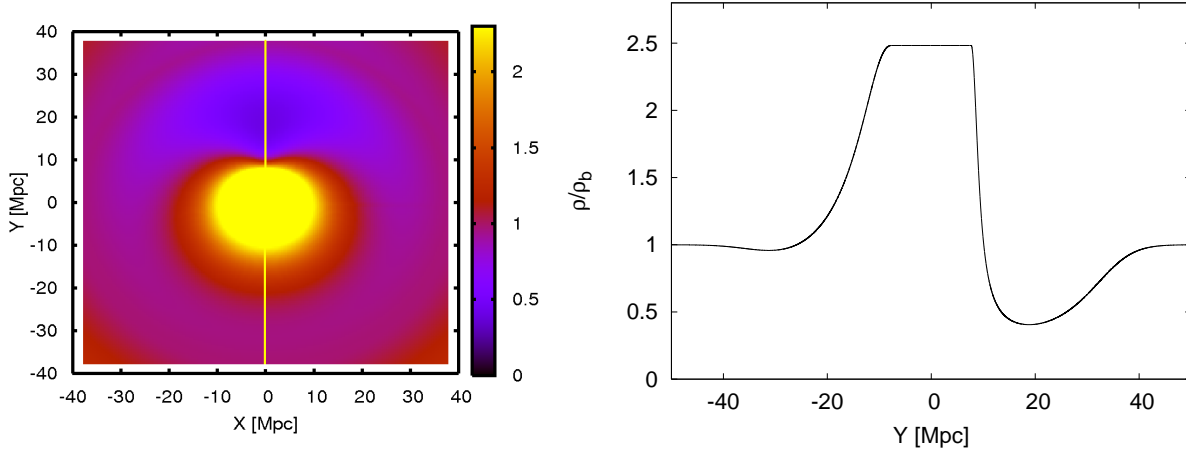


Figure 2: The density distribution ρ/ρ_b in region b at the present instant. The left panel presents the colour coded graph of density distribution in the surface $Z = 0$. The right panel presents the density distribution along the line shown in the left panel.

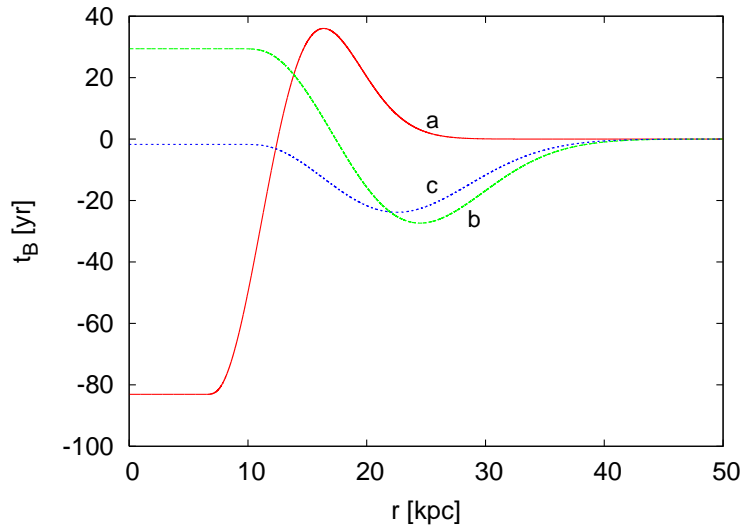


Figure 3: The bang time function $t_B(r)$ in regions a , b and c .

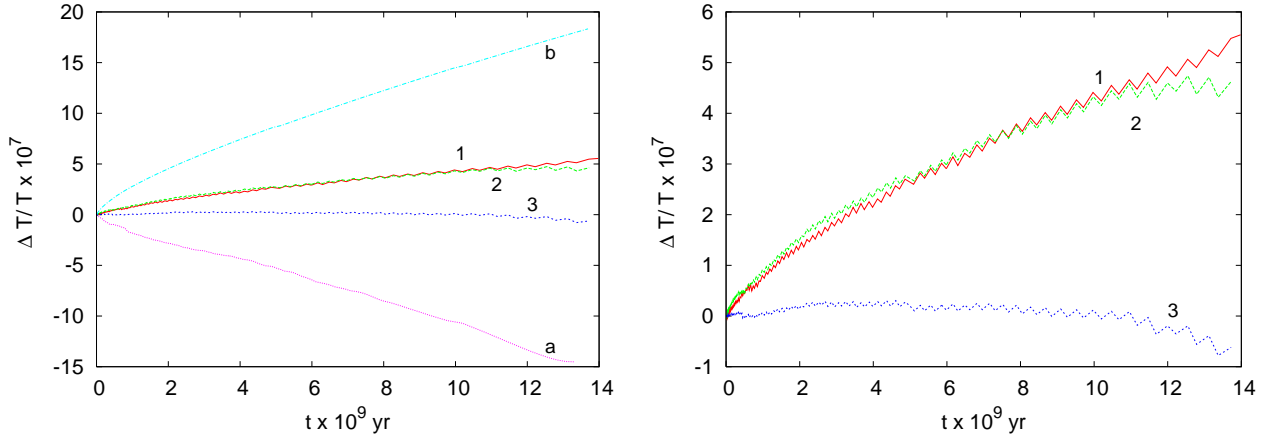


Figure 4: The temperature fluctuations caused by light propagation in models 1, 2, and 3 (detailed descriptions of these models are given in Sec. 5). Curve *a* presents temperature fluctuations obtained in the model where light propagated only through regions *a*. Curve *b* – light propagated only through regions *b*.

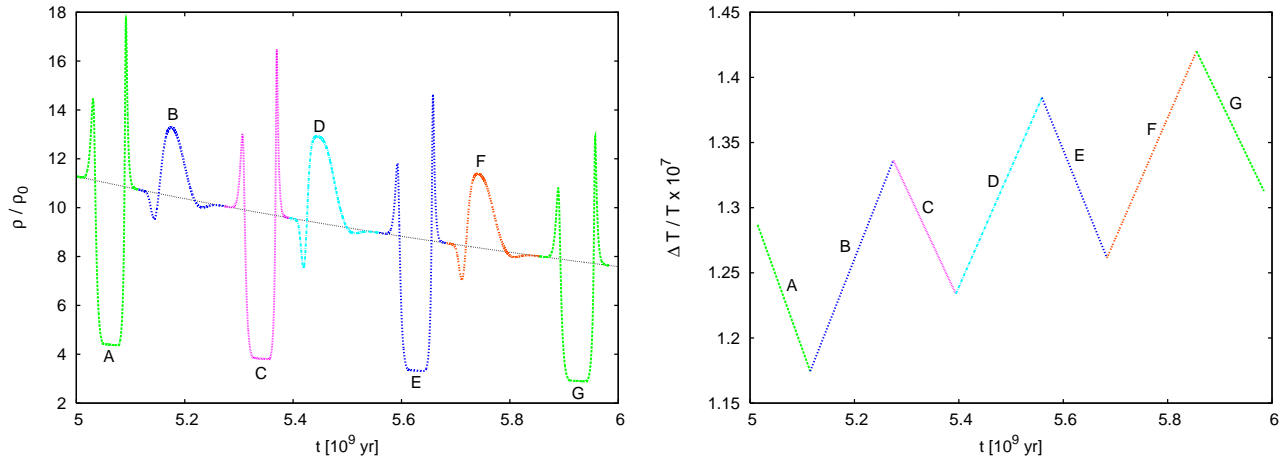


Figure 5: A small part of light propagation in model 1. The left panel presents the density variation that light ‘feels’ as it propagates. The black thin dotted line shows the density in the background model. The right panel presents the temperature fluctuations as measured by an observer situated outside the structure in the homogeneous region. Letters in the right panel label the temperature fluctuations caused by structures marked in the left panel by the same letters.

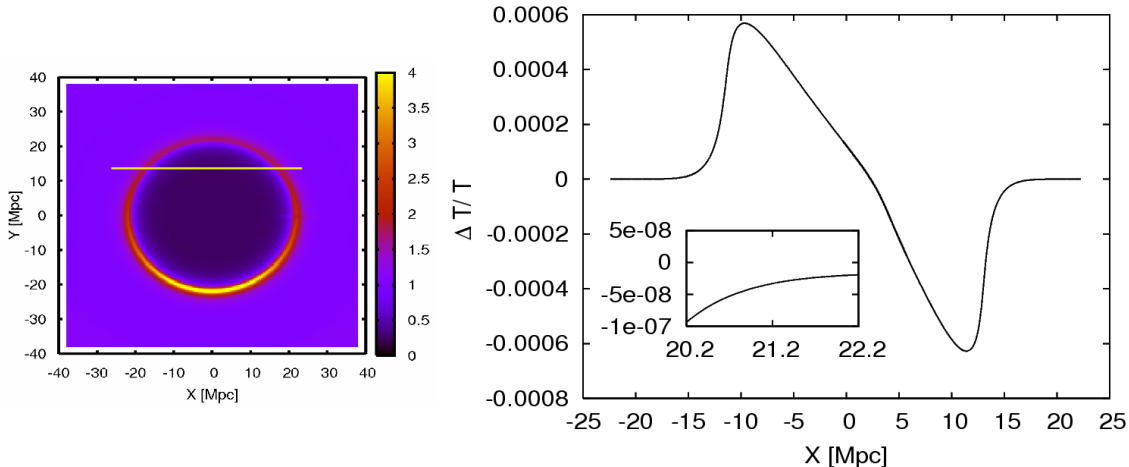


Figure 6: Right panel presents temperature fluctuations as measured by an observer along the path of light, which is presented by the yellow line in the left panel.

i.e. where the universe is homogeneous. However in the real Universe there is no place where an observer could say that the neighbouring structures are fully compensated and therefore the Universe nearby the observer can be treated as homogeneous. Since all measurements are always local, let us consider what happens if temperature fluctuations are measured in an uncompensated region. Fig. 6 presents the temperature fluctuations measured by an observer situated at different places within region a . The results presented in Fig. 6 are obtained under the assumption that light from the last scattering instant is propagating through homogeneous regions and currently reaches an observer in an inhomogeneous structure (region a). The light enters and propagates along the yellow line shown in the left panel of Fig. 6. $\Delta T/T$ fluctuations as measured along the ray's path are presented in the right panel of Fig. 6. These fluctuations are caused by the gravitational frequency shift — the differences between the densities inside and outside the structure — and by the Doppler effect — the difference between the expansion rates inside and outside the structure. If the structure were symmetric and did not evolve, then the frequency shift that appeared when light entered the structure would be cancelled by the opposite frequency shift on exit. Since the structure is not symmetric and it evolves, when light exits the structure the temperature fluctuations are not equal to zero. Inside the structure the temperature fluctuations caused by these effects are larger, and can reach, as seen in Fig. 6, even $\Delta T/T = 10^{-3}$.

The above results show that local structures can significantly contribute to the CMB temperature fluctuations. Thus it is important to test if local structures can be responsible for the observed correlations of the dipole, quadrupole and octopole axes of angular power spectrum of the CMB temperature fluctuations [7, 8, 9, 10, 11, 12].

6 Conclusions

The analysis presented in this paper aimed at examining the influence of light propagation effects on the temperature fluctuations of the CMB. Except for the Sunyaev–Zel'dovich effect (scattering of CMB photons on a ionised gas), the temperature fluctuations after the last scattering are caused by the gravitational frequency shift and the Doppler effect. The gravitational frequency shift is caused by the difference between potential energies inside and outside cosmic structures. The Doppler effect is due to different expansion rates inside and outside cosmic structures.

The above results imply that the Rees-Sciama effect caused by cosmic structures contributes to the temperature fluctuations as much as $10^{-6} - 10^{-7}$. This is smaller than the Sachs–Wolfe effect caused by inhomogeneities at the last scattering. However, if measurements are carried out inside inhomogeneous noncompensated structures, the amplitude of measured temperature fluctuations can be slightly higher. Therefore, it seems that, except for the Sunyaev–Zel'dovich effect, the largest contribution to the CMB temperature fluctuations is from the initial conditions at the last scattering and from our local cosmological vicinity.

Acknowledgements

I would like to thank Andrzej Krasinski for his help with preparing the manuscript and express my great gratitude to Peter and Patricia Gruber for their Fellowship. This research has been partly supported by Polish Ministry

of Science and Higher Education under grant N203 018 31/2873, allocated for the period 2006-2007. The Polish Astroparticle Network (621/E-78/SN-0068/2007) is also gratefully acknowledged for the financial support.

References

- [1] P. Szekeres, *Commun. Math. Phys.* **41**, 55 (1975).
- [2] C. Hellaby, *J. Math. Phys.* **37**, 2892 (1996).
- [3] P. J. E. Peebles, *The Large-Scale Structure of the Universe* (Princeton University Press, 1980).
- [4] C. L. Bennett et al., *Astrophys. J. Suppl. Ser.* **148**, 1 (2003).
- [5] C. Hellaby A. and Krasiński, *Phys. Rev.* **D66**, 084011 (2002).
- [6] W. B. Bonnor, *Commun. Math. Phys.* **51**, 191 (1976).
- [7] D. J. Schwarz, G. D. Starkman, D. Hutnerer, and C. J. Copi, *Phys. Rev. Lett.* **93**, 221301 (2004).
- [8] C. Vale, arXiv:astro-ph/0509039 (2005)
- [9] K. Land and J. Magueijo, *Phys. Rev. Lett.* **95**, 071301 (2005)
- [10] K. Land and J. Magueijo, arXiv:astro-ph/0611518 (2006)
- [11] A. Rakić, S. Räsänen, and D. J. Schwarz, *Mon. Not. R. Astron. Soc.* **369**, L27 (2006).
- [12] A. Rakić and D. J. Schwarz, arXiv:astro-ph/0703266 (2007)